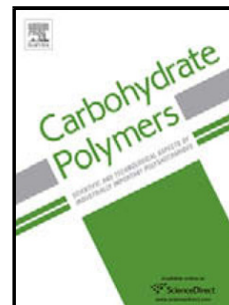


## Accepted Manuscript

Title: Morphology and Mechanical Properties of Poly(ethylene brassylate)/Cellulose Nanocrystal composites

Authors: Amaia Butron, Olatz Llorente, Jorge Fernandez, Emilio Meaurio, Jose-Ramon Sarasua



PII: S0144-8617(19)30612-5  
DOI: <https://doi.org/10.1016/j.carbpol.2019.05.091>  
Reference: CARP 14961

To appear in:

Received date: 27 February 2019  
Revised date: 30 May 2019  
Accepted date: 31 May 2019

Please cite this article as: Butron A, Llorente O, Fernandez J, Meaurio E, Sarasua J-Ramon, Morphology and Mechanical Properties of Poly(ethylene brassylate)/Cellulose Nanocrystal composites, *Carbohydrate Polymers* (2019), <https://doi.org/10.1016/j.carbpol.2019.05.091>

This is a PDF file of an unedited manuscript that has been accepted for publication. As a service to our customers we are providing this early version of the manuscript. The manuscript will undergo copyediting, typesetting, and review of the resulting proof before it is published in its final form. Please note that during the production process errors may be discovered which could affect the content, and all legal disclaimers that apply to the journal pertain.

**Morphology and Mechanical Properties of Poly(ethylene  
brassylate)/Cellulose Nanocrystal composites.**

Amaia Butron\*<sup>1,2</sup>, Olatz Llorente<sup>2</sup>, Jorge Fernandez<sup>3</sup>, Emilio Meaurio<sup>2</sup>, Jose-Ramon  
Sarasua<sup>2</sup>

<sup>1</sup>Tecnalia, Sede Azpeitia, Área Anardi 5, E-20730 Azpeitia - Gipuzkoa (Spain)

<sup>2</sup>Department of Mining-Metallurgy Engineering and Materials Science, POLYMAT,  
University of The Basque Country (UPV/EHU), School of Engineering, Plaza  
Ingeniero Torres Quevedo s/n, 48013 Bilbao, Spain

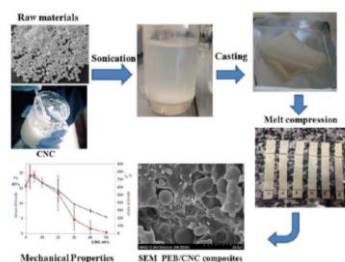
<sup>3</sup>Polimerbio, Paseo Mikeletegi 83, 20009 Donostia-San Sebastian, Spain

\* Corresponding author.

Phone: 647402336

Email: [amaia.butron@tecnalia.com](mailto:amaia.butron@tecnalia.com) (A. Butron)

## Graphical abstract



## Highlights

- Low CNC contents improve the mechanical properties of Poly(ethylene brassylate).
- Adding 2.5 wt% CNCs increases Young modulus by 14% and elongation at break by 23%.
- SEM images reveal the formation of a percolating network for the sonicated CNCs.
- High CNC contents improve the Young modulus at the expense of ductility.

## Abstract

Poly(ethylene brassylate), a novel inexpensive biodegradable polyester, has been reinforced with cellulose nanocrystals (CNCs) with the aim of improving its thermal stability and mechanical properties. The composites have been characterized through calorimetry, tensile tests, thermogravimetry and electron microscopy. The addition of small amounts of CNCs improves both the stiffness and the ductility of the composites, suggesting the existence of some compatibilizing effect. Adding large CNC amounts increases the Young modulus (e.g., 150% for 50 wt% CNCs), but now the material shows brittle behavior. Degradation of the CNCs starts at lower temperature suggesting mutual reactivity. The SEM analysis of the composites with ductile behavior reveals the formation of a percolating network crossing through the interconnected domains that conform a PEB-rich continuous phase. Processing consisting on reinforcement dispersion by sonication followed by melt processing results in composites in which the improvement of mechanical properties does not involve any trade-off.

**Keywords:** Poly(ethylene brassylate) (PEB); Cellulose Nanocrystals (CNC); Nanocomposites; Mechanical Properties.

## 1. Introduction

Conventional filled polymers, characterized by reinforcing fibers having diameters in the micrometer range, are currently being superseded by polymer nanocomposites (PNCs) containing homogeneously dispersed nanometric particles (Kumar, Benicewicz, Vaia, & Winey, 2017). Reducing particle size increases the specific surface area of the reinforcement up to the 150-170 m<sup>2</sup>/g range in case of nanocelluloses and to as much as 750 m<sup>2</sup>/g for nanoclays (Pranger & Tannenbaum, 2008). In addition, evenly dispersed nanoparticles also lead to the immobilization of the matrix polymer at the nanoparticle surface. As a result, compared with conventional composites, PNCs exhibit superior thermal, mechanical and barrier properties with lower reinforcing loads (1-5 vol%) and superior lightness, enabling thus greater retention of the inherent processability and toughness of the neat resin (Vaia & Wagne, 2004). For example, it has been shown that less than 5 vol% of exfoliated montmorillonite in nylon-6 increases the modulus by a factor of ~3 and raises the heat deflection temperature from ~340 to ~420 K (Kumar, Benicewicz, Vaia, & Winey, 2017; Ji, Jing, Jiang, & Jiang, 2002). Unfortunately, the high surface area of the nanoparticles also represents a significant processing challenge, because the van der Waals attraction between particles and the high viscosity of the matrix polymer makes it difficult to produce uniform dispersions of the nanoparticles throughout the matrix (Pranger & Tannenbaum, 2008).

Biodegradable PNCs are an ideal choice for biomedical applications based on biodegradable polymer matrices requiring improved mechanical properties, such as implants, bone cements or drug delivery systems. Among the biodegradable polymer matrices, high molecular weight poly(ethylene brassylate) (PEB) has been recently synthesized by Mecerreyes et al. (Pascual, Sardon, Veloso, Ruipérez, & Mecerreyes, 2014). The ethylene brassylate (EB) monomer is a 17 member ring lactone commercially available and cheaper than lactide,  $\epsilon$ -caprolactone and other macrolactones. The EB monomer can be easily synthesized from castor oil renewable source (extracted from Castor plant). The methylene/ester ratio in the repeat unit of PEB [-O-CO-(CH<sub>2</sub>)<sub>11</sub>-CO-O-(CH<sub>2</sub>)<sub>2</sub>-] is only slightly larger than that of poly( $\epsilon$ -caprolactone) (PCL). The PEB homopolymer presents similar properties to PCL, but with slightly higher melting ( $T_m$  ~ 70 °C compared to ~ 60 °C for PCL) and glass transition

temperatures ( $T_g \sim -30\text{ }^\circ\text{C}$  compared to  $T_g \sim -60\text{ }^\circ\text{C}$  in PCL) and good thermal stability (Cama, Mogosanu, Houben, & Dubruel, 2017; Fernández, et al., 2016; Fernández, Montero, Etxeberria, & Sarasua, 2017; Fernández, Larrañaga, Etxeberria, & Sarasua, 2016).

On the other hand, though celluloses have been used for nearly 150 years, over these last decades interest in this material has been reawakened because of its abundance, low cost, renewable nature and exceptional mechanical properties (Lizundia, Meaurio, & Vilas, 2016). Nanocelluloses are currently classified into five broad categories: cellulose nanocrystals (CNCs), cellulose nanofibrils (CNFs), tunicate CNCs (t-CNCs), algal cellulose (AC), and bacterial cellulose (BC) (Foster, et al., 2018). The first nanocelluloses were actually obtained from wood or plants (such as cotton), and were refined using two major procedures: acid hydrolysis and mechanical shear, leading respectively to CNCs and CNFs. Cellulose nanocrystals (CNCs) are often referred to as whiskers, nanowhiskers, needles, nanocrystals and nanoparticles (Habibi, Lucia, & Rojas, Cellulose Nanocrystals: Chemistry, Self-Assembly, and Applications, 2010.). The main process used to prepare CNCs is acid hydrolysis, which hydrolyzes the cellulose (removing the amorphous parts and releasing the microfibrils at the defects) to produce rod-like cellulose nanocrystals (Foster, et al., 2018; Lin & Dufresne, 2014). This process also introduces sulfate half ester groups in the CNC surfaces that stabilize the colloidal suspensions in water environment (Foster, et al., 2018). When the cellulose source is trees/plants (e.g., wood or cotton), the released nanoparticles (CNCs) present a diameter of 5–20 nm, and typical lengths in the 50–350 nm range (Foster, et al., 2018). Regardless of the source, CNCs are elongated needle-like nanoparticles, and each rod can be considered a rigid cellulosic crystal with no apparent defect (Lin & Dufresne, 2014). On the other hand, Cellulose Nanofibrils (CNFs), also termed nanofibrillar celluloses, cellulose nanofibers, cellulose microfibrils and microfibrillar celluloses are typically refined using mechanical shear, aided with other treatments such as oxidation reactions or enzymatic processes (Xu, et al., 2013). Contrarily to CNCs, CNFs contain amorphous cellulose regions linking the cellulose crystals to form long, flexible, fiber networks with a fibril diameter similar to or larger than CNCs (Lin & Dufresne, 2014; Xu, et al., 2013). The length of the CNFs is hard to define due to the network structure and is seldom reported (Lin & Dufresne, 2014). Recently, tunicates, algae and bacteria have been explored as nanocellulose sources, and have been

classified in separate groups due to the unique characteristics of the nanocelluloses obtained. However, these new sources are processed using the same essential refinement procedures as above, resulting in CNC-like or CNF-like materials. For example, Bacterial Celluloses (BCs) are synthesized by bacteria in a pure form, and are hence a convenient source to obtain CNFs because intensive processing to remove unwanted impurities such as lignin, pectin and hemicellulose is unnecessary (Lin & Dufresne, 2014; Lee, et al., 2012). They are usually classified as a separate nanocellulose class because of its differential characteristics, such as a ultra-fine network of cellulose nanofibers, higher polymerization degrees of the cellulose chains and higher crystallinity (60-90%) (Lin & Dufresne, 2014; Chen, Cho, & Jin, 2010). Regardless of the source, CNFs are usually processed in water suspension (or in the desired solvent suspension after stepwise transferal) without drying the nanocellulose fibers (Peng, Gardner, & Han, 2012; Clasen, Sultanova, Wilhelms, Heisig, & Kulicke, 2006; Beaumont, König, Opietnik, Potthast, & Rosenau, 2017). Drying CNFs usually results in an irreversible aggregation of fibers termed hornification, where large numbers of hydrogen bonds are formed between the hydroxyl groups on adjacent fibrils (Clasen, Sultanova, Wilhelms, Heisig, & Kulicke, 2006). As a consequence, the nanocellulose loses porosity and reinforcing ability. In contrast, the extent of hornification of CNCs is limited compared to CNFs (Mihrianyan, 2011), hence, CNCs are commercially available as redispersible freeze/spray dried powders (Foster, et al., 2018; Khoshkava & Kamal, 2014). Regarding the reinforcing ability, never dried CNFs are superior to CNCs due to their network structure and larger aspect ratios (Xu, et al., 2013; Lee, et al., 2012).

This paper investigates novel PNCs based on renewable biobased materials, namely Poly(ethylene brassilate) (PEB) and Cellulose Nanocrystals (CNCs). The reinforcing CNC particles have been dispersed by sonication, followed by solvent casting. The final PNC slabs have been obtained by melt pressing of the solvent-cast PNC films. The thermal and mechanical properties have been then investigated through DSC and tensile tests, and the results have been discussed considering the images obtained by electron microscopy. Finally, the degradation behavior of the samples has been analyzed by TGA.

## 2. Experimental Section

### 2.1 Materials

Ethylene Brassylate monomer (purity > 95%) was supplied by Sigma Aldrich, and was polymerized using bismuth triphenyl (Ph<sub>3</sub>B) obtained from Gelest as catalyst and 1-Hexanol as initiator. The resulting polymer was purified by solution/precipitation in the chloroform/methanol system. Its molecular weight ( $M_w = 230$  kg/mol) and dispersity ( $D = 2.3$ ) were determined by GPC using a Waters 1515 GPC device equipped with two Styragel columns ( $10^2 - 10^4$  Å) using Chloroform as eluent (Fernández, et al., 2016; Fernández, Montero, Etxeberria, & Sarasua, 2017).

Wood-based CNCs were purchased from Alberta Innovates - Technology Futures (AITF). The CNCs were produced on the pilot scale plant (production capacity up to 100 kg of CNC per week) located in Edmonton, Canada (Ngo, Danumah, & Ahvazi, 2018; George, Shen, Sharma, & Montemagno, 2017). Softwood pulp was used as cellulose source, and typical hydrolysis conditions were 63.5 wt% sulfuric acid at 45 °C for 2 h. Water reverse osmosis was used to quench the hydrolysis, and then CNCs were neutralized to sodium form using NaOH. The size of the rod-like CNC particles is about 100-200 nm in length and 5-10 nm in diameter (Reid, Villalobos, & Cranston, 2017; Bayati, Boluk, & Choi, 2014), and were received in spray-dried form.

### 2.2 Composite Preparation

Films of the PEB/CNC composites were prepared with CNC compositions ranging from 2.5 to 50 wt%. At least 4 films were obtained for each composition. A constant volume of chloroform (20 ml) was used to disperse the appropriate amount of CNCs without exceeding the saturation limit (0.25 g. CNC/20 ml CHCl<sub>3</sub>). Sonication was carried out for 15 min. in a Vibra Cell 75115 sonicator equipped with a CY33 probe operating at 40 kHz. The appropriate amount of PEB was then added to the sonicated solutions and allowed to dissolve with the aid of a vortex mixer. Since the solution polymer concentration was limited in all cases to 5 wt%, solutions with CNC contents below the saturation limit were required to prepare the PEB-rich composites. As illustrative examples, the composite containing 50 wt% CNCs was prepared mixing 0.25 g CNCs with 0.25 g PEB, while the one containing 2.5 wt% CNCs was prepared from 0.0256 g CNCs and 1 g. PEB. To obtain films of uniform thickness, the cast film composites

were processed by melt compression at 175 °C and 250 bar for 15 seconds in a Collin P 200 hydraulic press. Then, the molds were slowly cooled to 35 °C to ensure correct crystallization.

### **2.3 DSC**

Melt pressed films were analyzed by Differential Scanning Calorimetry (DSC) in a Q2000 model from TA Instruments. Two different samples for each composition weighing between 6 and 9 mg were cut from the films, encapsulated in aluminum pans, and scanned from room temperature to 130 °C at 20 °C/min. They were then cooled to -80 °C to perform a second heating scan from -80 °C to 130 °C at 20 °C/min. Glass transition temperatures ( $T_g$ ) were determined as the midpoint temperature of the specific-heat jump from the glassy to the liquid state.

### **2.4 Tensile Tests**

The mechanical properties at room temperature ( $21 \pm 2$  °C) were determined by tensile tests with an Instron 5565 testing machine at a crosshead displacement rate of 10 mm  $\text{min}^{-1}$  following ISO 527-3/1995 standard. Specimens 80 mm length and 10 mm wide were cut from films 250–400  $\mu\text{m}$  thick and tested with a distance of 50 mm between marks. The mechanical properties reported are the Young modulus, stress at yield, strain at yield, ultimate tensile stress and elongation at break) correspond to average values of at least 5 determinations.

### **2.5 Thermogravimetry**

To study the thermal degradation of the composites, a Thermogravimetric Analysis (TGA) was made. The results are presented as mass loss curves and their derivative curves. The equipment used in this study is the TGA Q50-0545 from TA Instruments. Sample weights were in the 10 - 15 mg range in ceramic crucibles from 25 to 700 °C at a rate of 5 °C/min.

### **2.6 Electron Microscopy (SEM and TEM)**

To study the morphology of the composites, Cryofractured samples have been analyzed in a Hitachi S-4800 cold-cathode field-emission scanning electron microscope (FE-SEM) at an acceleration voltage of 15 kV, achieving resolutions on the order of 1 nm in these operating conditions. The dry samples were cryogenically frozen, cut, and gold-

coated (15 nm thick coating) in an Emitech K550X Sputter Coater to obtain cross-section images.

CNC dispersion was evaluated using Transmission Electron Microscopy (TEM) on a TECNAI G2 20 TWIN operated at 120 kV and equipped with LaB6 filament. The dried films of about 80 nm of thickness were obtained at -70 °C using an ultramicrotome device (Leica EMFC6) equipped with a diamond knife. The ultrathin sections were placed on 200 mesh copper grids.

### 3. Results and Discussion

#### 3.1. DSC Analysis

Figure 1 shows the heat flow in the first DSC scans for the samples containing 0, 2.5, 5, 10, 15, 20, 30, 40 and 50 wt% CNCs. As can be seen, all the curves show an endothermic peak at about 70 °C corresponding to melting of PEB. The second scans (from -80 °C to 130 °C, not shown) also show a specific heat jump at about -30 °C corresponding to the glass transition temperature of PEB. Table 1 lists the glass transition temperature ( $T_g$ ), the heat-capacity jump at the glass transition temperature ( $\Delta c_p$ ), the melting temperature ( $T_m$ ) and the melting enthalpy ( $\Delta H_m$ , normalized to the PEB content) of pure PEB and the PEB/CNC composites. As can be seen, the glass transition temperature is almost unaffected by the addition of the CNCs, in agreement with the behavior observed in most studies in this field (Habibi, Lucia, & Rojas, Cellulose Nanocrystals: Chemistry, Self-Assembly, and Applications, 2010.; Dufresne, 2017). This result suggests the absence of nanoconfinement effects that usually increase the  $T_g$  of the PNCs (Qin, Xia, Sinko, & Keten, 2015; Dong, et al., 2012). Moreover, the melting temperature and the normalized  $\Delta H_m$  do not decrease with composition, suggesting that the dispersion of the CNCs does not decrease the size of the crystallites. Both results suggest a poor dispersion of the CNCs (Roohani, et al., 2008).

Regarding the melting temperature, our results indicate an increase of about 3-4 °C with the addition of CNCs. To explain this result, it must be recalled that many polyesters such as PCL or poly(p-dioxanone) usually show a double melting behavior, attributed to melting, recrystallization and subsequent remelting during the DSC scan (Lezcano, Salom Coll, & Prolongo, 1996; Pezzin, Alberda van Ekenstein, & Duek,

2001; Sanchez-Rexach, Martínez de Arenaza, Sarasua, & Meaurio, 2016). The lower temperature contribution (LTm) is attributed to the initial crystals existing in the sample, while the higher melting point (HTm) is attributed to the crystals formed during the recrystallization process occurring after melting of the initial crystals. In case of PEB, both peaks appear highly overlapped (resembling those of PCL), and the nucleating effect of the CNCs should speed up the recrystallization process, increasing the intensity of the recrystallization peak and shifting the Tm to higher temperatures.

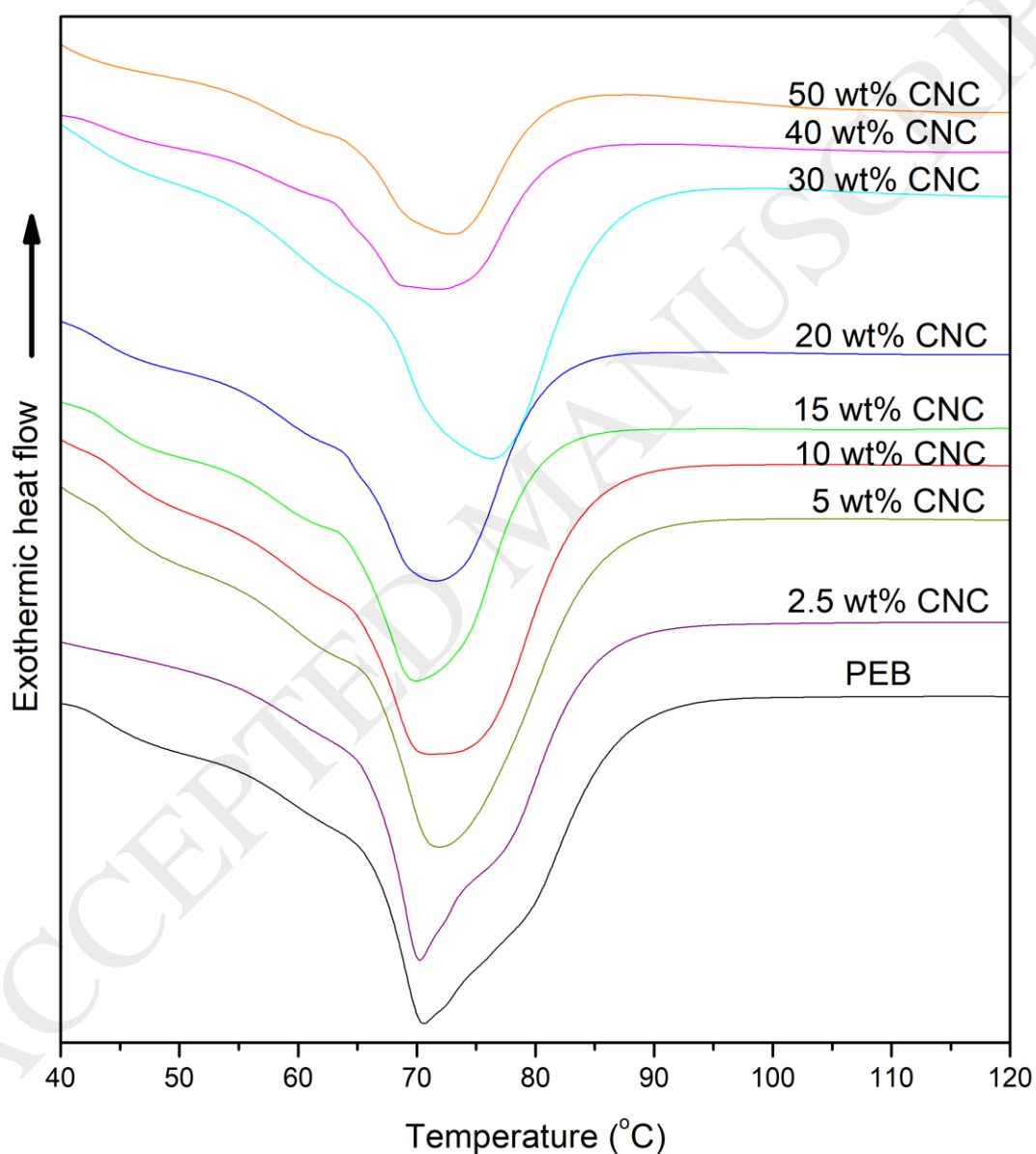


**Figure 1.** First DSC scans. Melting enthalpies (exothermic heat flow against temperature) for PEB, CNC and PEB/CNC composites.

**Table 1.** Glass transition temperature, specific heat jump, melting temperature and melting enthalpy normalized to the weight of PEB for the different PEB/CNC composites obtained from the second DSC scans.

CNC wt%	T <sub>g</sub> (°C)	Δc <sub>p</sub> (J/g)	T <sub>m</sub> (°C)	ΔH <sub>m</sub> (J/g)
0	-28.9	0.313	69.7	90.7
2.5	-27.5	0.309	69.9	94.4
5.0	-27.1	0.296	72.9	95.0
10	-28.7	0.259	72.5	92.5
15	-29.1	0.250	70.3	92.9
20	-29.0	0.243	70.9	94.8
30	-28.4	0.160	75.7	89.0
40	-29.5	0.158	72.1	92.0
50	-29.9	0.120	73.8	89.3

### 3.2. Mechanical Properties of PEB/CNC Nanocomposites.

PEB is a flexible, ductile polymer that resembles the mechanical properties of PCL (Fernández, et al., 2016; Fernández, Montero, Etxeberria, & Sarasua, 2017) or low-density polyethylene (LDPE) (Lo Re, et al., 2018). High molecular weight PEB ( $M_w > 10^5$  g/mol) shows deformation at break ~900%, tensile strength ~26 MPa and yield point ~11 MPa (Fernández, et al., 2016; Fernández, Montero, Etxeberria, & Sarasua, 2017). Figure 2a shows the stress-strain curves obtained for the pure PEB and the PEB/CNC composites investigated in this work. As can be seen, adding small amounts of CNCs (up to 5 wt%) increases the ductility of pure PEB; but further addition of CNCs reverses this trend. Anyway, most of the ductility present in pure PEB is retained on composites with CNC loads up to 20 wt%, which achieve rupture elongations above 500%. However, composites with CNC loads over 30 wt% break soon after the yield point, showing fragile behavior. Fig. 2b is an expansion of the elastic region and the start of the plastic region. As can be seen, the addition of CNCs increases the slope of the elastic region, hence, the stiffness of the composites. In addition, plastic deformation starts at lower strains with the addition of CNCs, considerably reducing the area below the yield peak. The plastic region is much shorter in samples with CNC loads above 30 wt%.

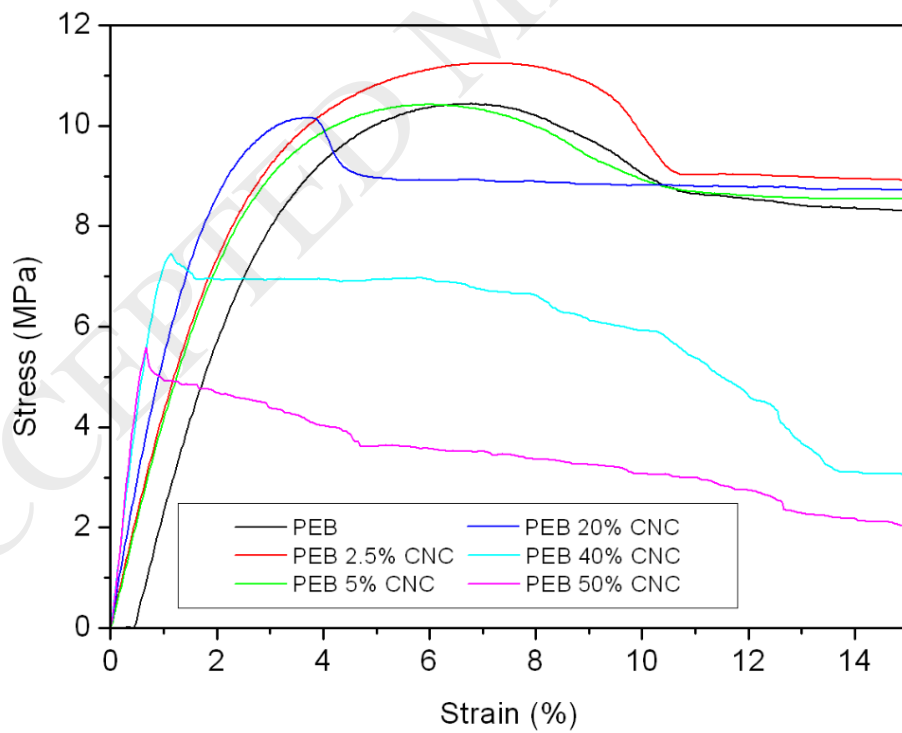
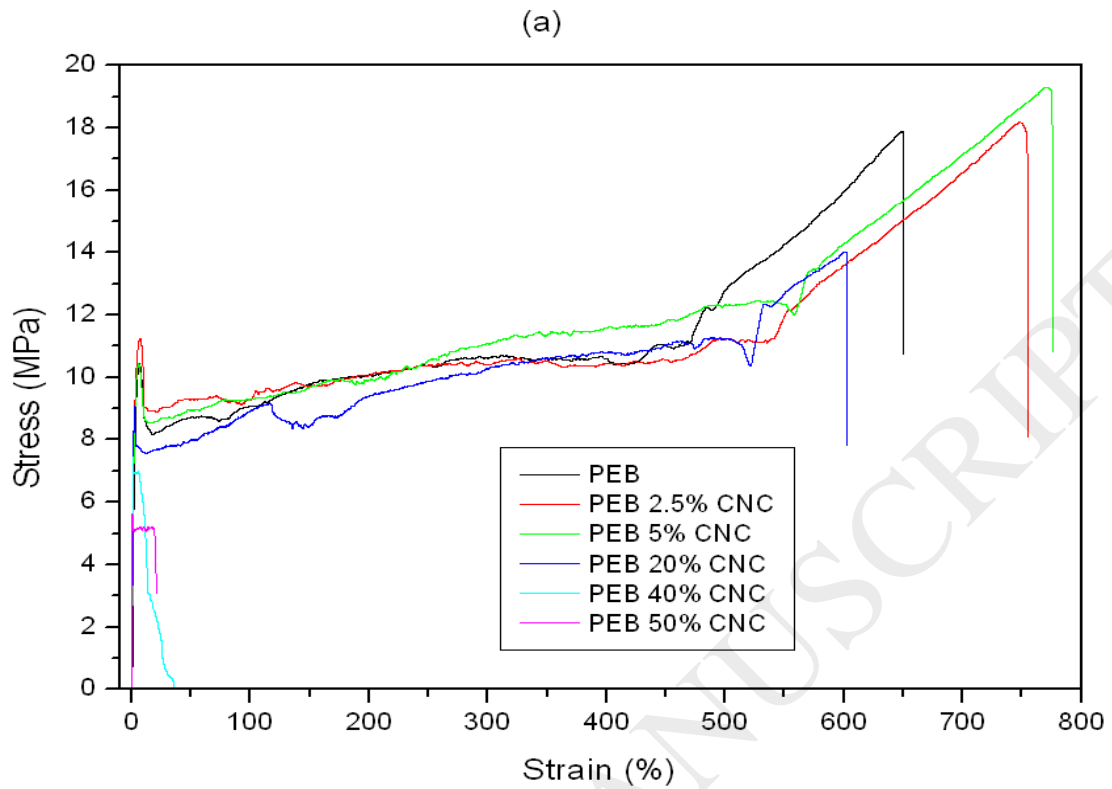


**Figure 2.** Stress-strain curves for the PEB/CNC composites. (a) Stress-strain curves, (b) expanded graph showing the elastic region and beginning of yield.

Figure 3 shows the elastic modulus ( $E$ ), the yield stress ( $\sigma_y$ ), the strain at yield ( $\epsilon_y$ ), the stress at break ( $\sigma_b$ ) and the strain at break ( $\epsilon_b$ ). As can be seen, the largest stiffening efficiency (or the largest increase in Young modulus relative to the CNC content) is obtained for the sample containing 2.5 wt% CNCs. In fact, the Young modulus of this composite is even larger than the one obtained after doubling the CNC content to reach 5 wt%. The large reinforcing efficiency observed at low concentrations is attributable to the homogeneous dispersion of the reinforcement, resulting in the largest possible interfacial area between the reinforcement and the matrix and, hence, the best transmission of stresses. Larger reinforcement contents result, however, in the formation of a rigid percolation network arising from hydrogen bonding interactions between neighboring whiskers (Azzi Samir, Alloin, & Dufresne, 2005; Ten, Bahr, Li, Jiang, & Wolcott, 2012). The percolation threshold ( $v_{Rc}$ , critical volume fraction of Rod-like particles) is related to the aspect ratio of the rod-like particles ( $L/d$ ) by:

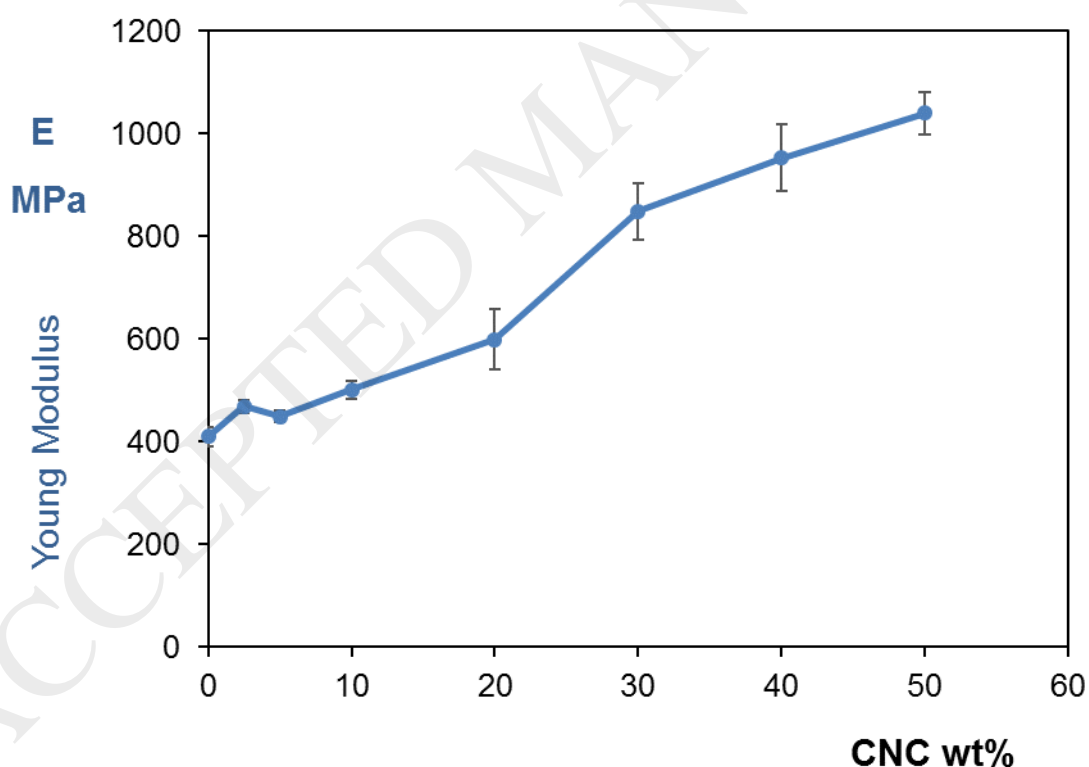
$$v_{Rc} = \frac{0.7}{L/d} \quad (1)$$

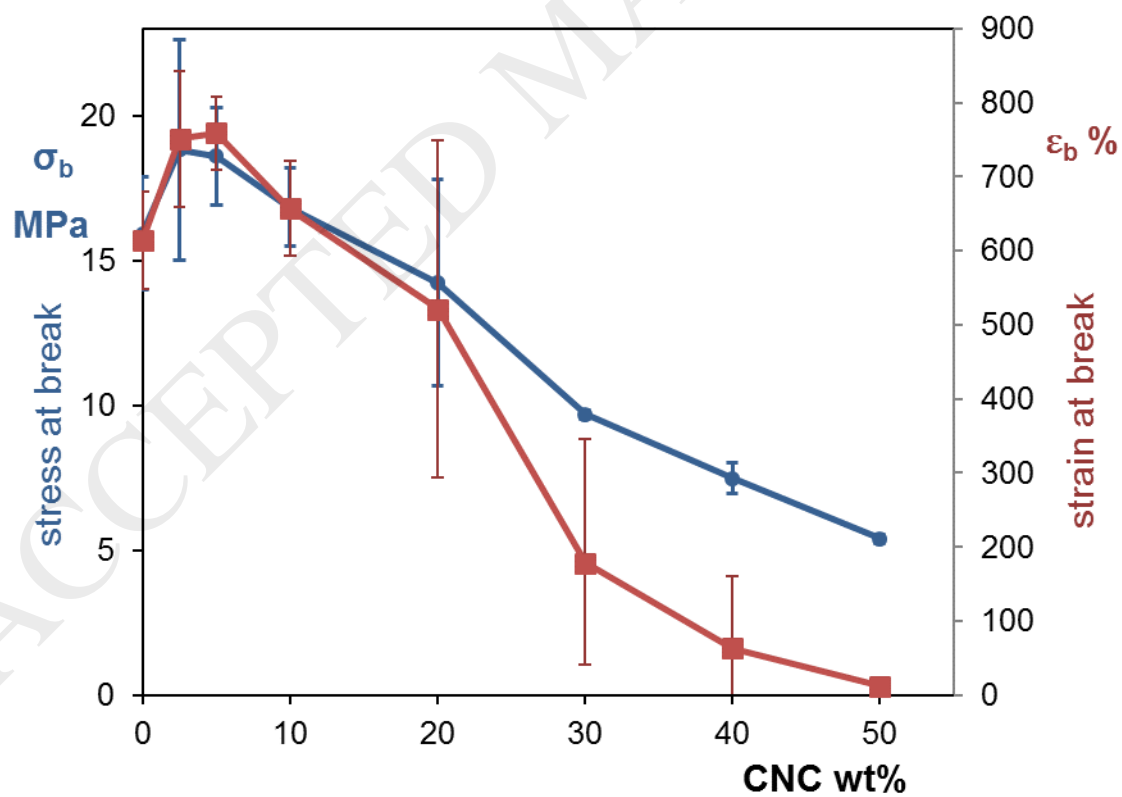
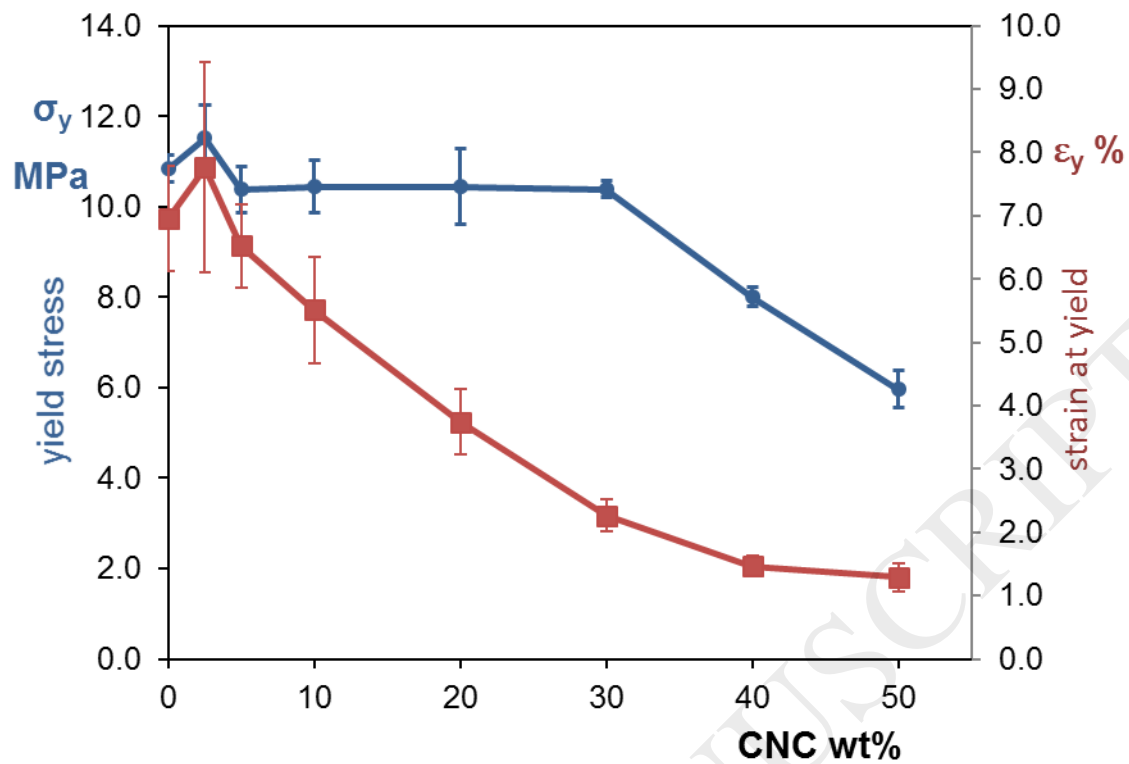
Considering the aspect ratio of the CNCs used in this work ( $L/d \sim 20$ , see experimental part), the percolation threshold is 3.5 vol%, or 4.7 wt% (taking into account the densities of PEB and CNCs, 1.1 and 1.5 g/cm<sup>3</sup> respectively). Hence, the loss of stiffness observed on going from 2.5 wt% CNCs to 5 wt% CNCs can be attributed to the formation of a percolation network, that decreases the interfacial area with the matrix (Azzi Samir, Alloin, & Dufresne, 2005; Ten, Bahr, Li, Jiang, & Wolcott, 2012). A similar behavior has been reported for other PNCs (Ten, Bahr, Li, Jiang, & Wolcott, 2012; Dhar, Tarafder, Kumar, & Katiyar, 2015). Of course, further addition of CNCs strengthens the percolation network and consequently the whole PNC, increasing the stiffness by a factor up to 2.5 for a 50 wt% CNC content.

Figure 3 also shows the yield stress and the strain at yield, obtained from the maximum occurring at the end of the initial linear (elastic) region of the stress-strain curves. As can be seen, the maximum reinforcing efficiency is again achieved when the amount of CNCs is below the percolation threshold. In the concentration regime at which nanoparticle aggregation is expected, the strain at yield is observed to decrease continuously with the addition of CNCs, but the stress at yield is still able to retain a

value close to that of the pure polymer up to 30 wt% CNC contents. CNC contents above this value result in a considerable reduction of the yield stress, indicating a decrease of the resistant properties of the material.

The last chart in Figure 3 shows the stress at break and the strain at break (the latter a good indicator of ductility) for the PEB/CNC nanocomposites. As can be seen, the addition of CNCs up to the percolation limit also increases the ductility of the samples. This result makes the PEB/CNC system particularly interesting since in most cases the addition of CNCs improves the resistant properties *at the expense* of the ductility of the sample (Habibi, Lucia, & Rojas, Cellulose Nanocrystals: Chemistry, Self-Assembly, and Applications, 2010,; Siqueira, Bras, & Dufresne, 2009). Even more, the nanocomposites retain high toughness with CNC contents up to 20 wt%. Above this value, toughness decreases drastically.





**Figure 3.** Selected mechanical properties for the PEB/CNC nanocomposites

In summary, the analysis of the mechanical properties shows that the largest reinforcing efficiency is obtained for a 2.5 wt% CNC content. In addition, it is particularly interesting to stress that the addition of CNCs improves all the mechanical properties of PEB, *including ductility*. For comparison, in the PCL/CNC system the addition of a small amount of CNCs, as low as 3 wt%, was found to cause a significant reduction of the strain at break (Siqueira, Bras, & Dufresne, 2009). Grafting the polymer onto the CNCs resulted in a better retention of ductility (Habibi, et al., 2008), or even in its improvement in specific cases (Yu, Qin, Yan, & Yao, 2014). In the PEB/CNC system investigated here, ductility is enhanced without a dedicated grafting stage. However, grafting reactions cannot be discarded in our system due to the possibility of transesterification reactions occurring during the melt processing step. In particular, intermolecular alcoholysis between the OH groups in cellulose and the ester groups in PEB might have grafted PEB chains on the surface of the CNCs (Yuan & Ruckenstein, 1998; Zuza, Meaurio, Etxeberria, & Sarasua, 2006), improving the compatibility of the system on correctly dispersed systems thanks to the previous sonication step (Jiang, Morelius, Zhang, Wolcott, & Holbery, 2008). In fact, the overall reinforcing effect is favorable even for composites with relatively large CNC contents of up to 20 wt%, since they show noticeably larger stiffness at the expense of a moderate-to-small decrease of ductility. Table 2 lists the mean values, and corresponding deviations, for the Young modulus (E), the stress at yield ( $\sigma_y$ ), the strain at yield ( $\epsilon_y$ ) and the strain at break ( $\epsilon_b$ ).

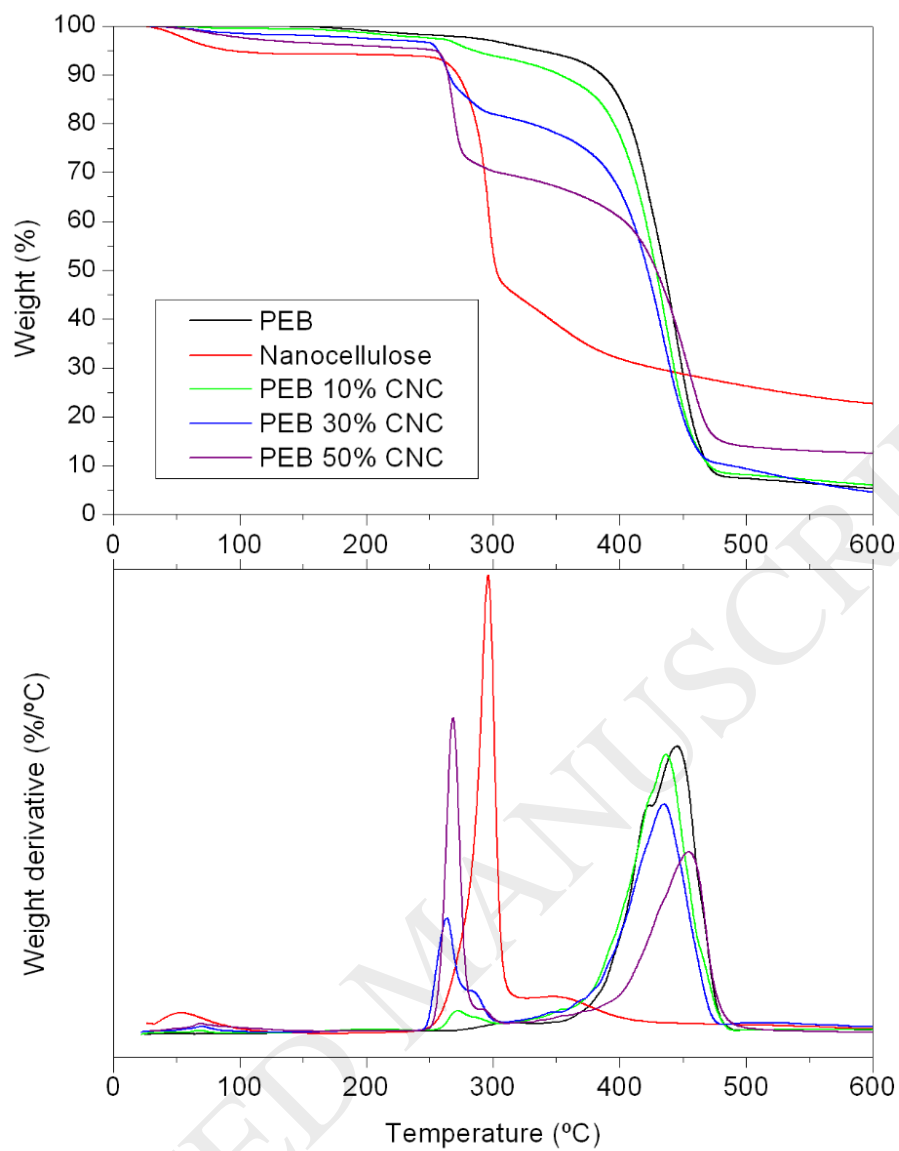
**Table 2.** Mechanical properties of different concentrations of CNC copolymers

CNC composition (wt%)	E (Mpa)	$\sigma_y$ (MPa)	$\epsilon_y$ (%)	$\epsilon_b$ (%)
PEB	410 ± 19	10.8 ± 0.3	7.0 ± 0.8	613 ± 66
2.5	469 ± 12	11.5 ± 0.7	7.8 ± 1.7	751 ± 92
5.0	448 ± 11	10.4 ± 0.5	6.5 ± 0.7	759 ± 50
10	501 ± 17	10.4 ± 0.6	5.5 ± 0.8	657 ± 64
20	599 ± 59	10.4 ± 0.8	3.7 ± 0.5	521 ± 228
30	849 ± 55	10.4 ± 0.2	2.3 ± 0.3	178 ± 168
40	952 ± 65	8.0 ± 0.2	1.5 ± 0.2	63 ± 61
50	1040 ± 40	6.0 ± 0.2	1.3 ± 0.2	13 ± 6

### 3.3. Thermal Stability of the PEB/CNC Nanocomposites

CNCs are obtained by means of a hydrolysis process (see experimental) that introduces sulfate groups in their surface. The presence of even a small amount of sulfate groups can cause a considerable decrease in the degradation temperature start, to as low as 150 °C (Roman & Winter, 2004). For this reason, low acid concentrations, low acid-to-cellulose ratios, and short reaction times are preferred (Roman & Winter, 2004). In addition, neutralization after the hydrolysis step is also required to improve the thermal stability of the CNCs (Habibi, et al., 2008). An alternative is to use hydrochloric acid, which does not introduce any acidic groups, but presents the disadvantage of the aggregation of the cellulose crystals due to the lack of surface charges. Figure 4 shows the thermogravimetric curves obtained for the PEB/CNC system investigated in this work. As can be seen, these CNCs show high thermal stability since their degradation does not start up to 250 °C (the small weight loss observed at low temperatures is attributable to the hygroscopicity of the samples), suggesting the presence of only a residual amount of neutralized sulfate groups in the pristine CNCs.

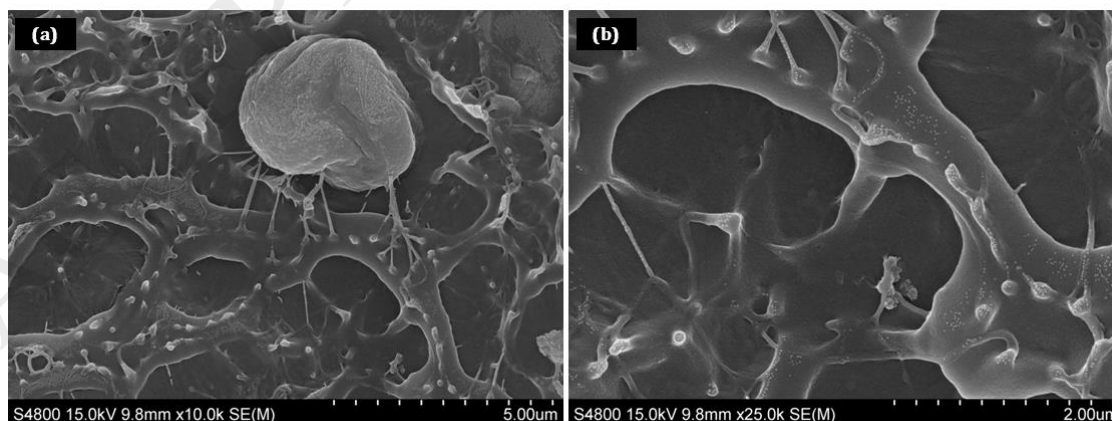
Regarding pure PEB, degradation of biodegradable polymers typically starts by depolymerization reactions, which are usually weight lossless. The weight loss rate maximum displayed by pure PEB at about 450 °C (see Figure 4), might correspond to the temperature at which the depolymerization products degrade to low molecular weight gases or, more simply, to the boiling temperature of the monomer. In other words, polymer degradation through the decrease of molecular weight probably occurs before the temperature corresponding to the peak observed in Figure 4. In the PEB/CNC composites, the addition of PEB to the CNCs reduces the degradation temperature of the CNCs by about 30 °C, suggesting that the transesterification reactions occurring between PEB and the CNCs might speed up the degradation of the CNCs. In spite of this small change, the thermogravimetric analysis suggests an almost additive behavior for the PEB/CNC nanocomposites.



**Figure 4.** Weight loss and its derivative for 0, 10, 30, 50 and 100 CNC wt%.

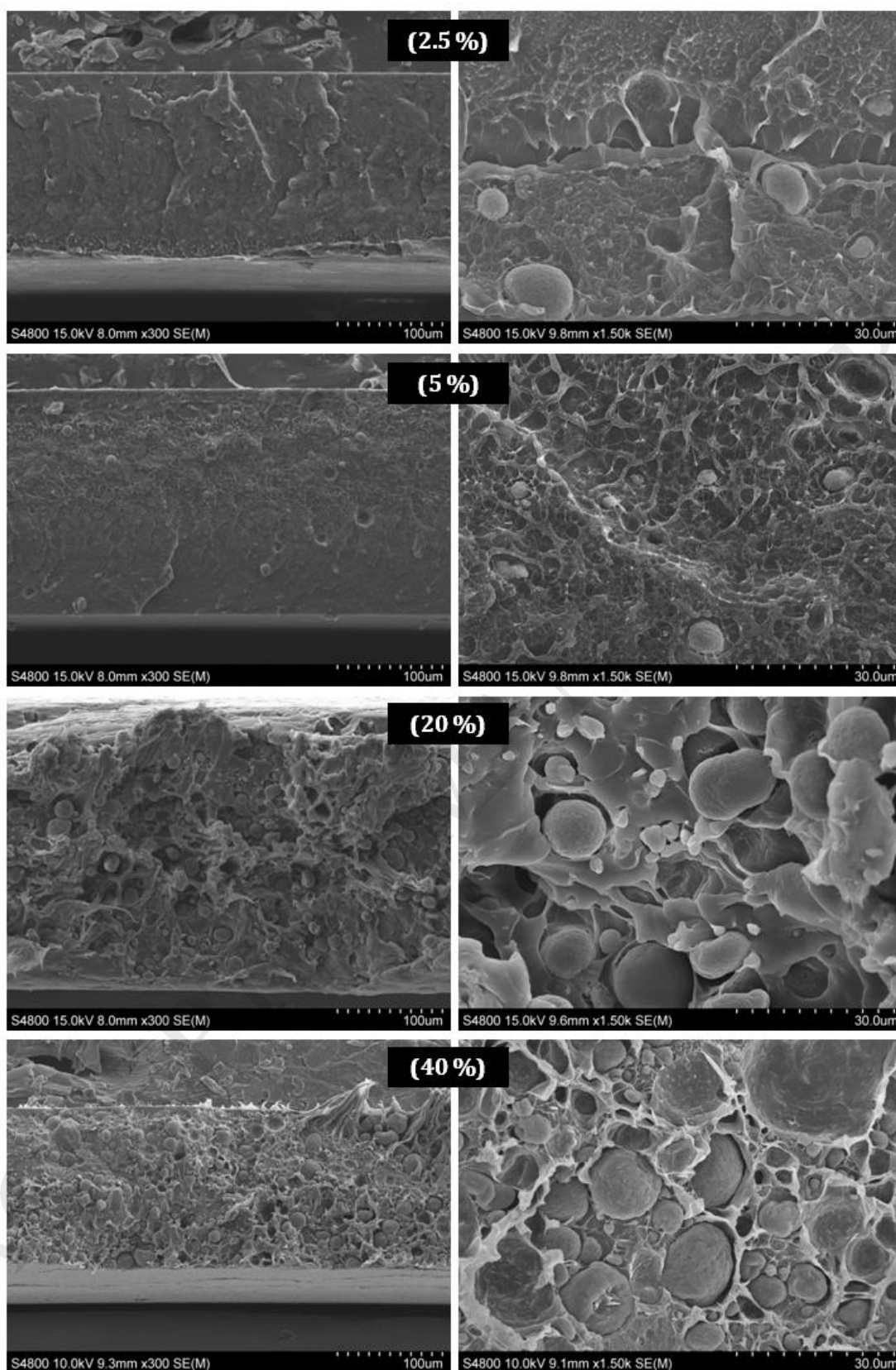
### 3.4. Electron Microscopy Analysis.

Figure 5 shows high magnification SEM micrographs obtained for the composites containing 5 wt% CNC, in which the CNCs appear as “spots” (Boujemaoui, et al., 2017; Hoeger, 2017). The presence of these white dots can be assigned to small CNC aggregates interconnected by the percolating rod-like CNCs, which can be observable in the event the CNCs come parallel to the rupture surface (see the upper part of Figure 5b). As can be seen in Figures 5a and 5b, the CNCs are not evenly dispersed, but form a rigid percolating network, resulting from the strong interactions between them (Habibi & Dufresne, Highly Filled Bionanocomposites from Functionalized Polysaccharide Nanocrystals, 2008). In addition, the spot-like appearance of the CNCs indicates that the reinforcing nanofibers are exposed to the surface rather than being embedded in the PEB matrix. This morphology of the rupture-surface suggests poor compatibility between the reinforcement and the polymeric matrix (Boujemaoui, et al., 2017). Smoother rupture surfaces without the "spots" present in Figure 5 can be achieved using dispersing strategies that improve the adhesion of the reinforcement with the polymeric matrix, such as graft polymerization, silylation of the -OH groups in cellulose, or the use of surfactants (Siqueira, Bras, & Dufresne, 2009; Habibi, et al., 2008; Boujemaoui, et al., 2017). Finally, the polymeric phase around the percolating network shows interconnected domains that result in a PEB-continuous phase.



**Figure 5.** SEM images of the PEB/CNC composite containing 5 wt% CNC with magnification 10000x (left) and 25000x (right).

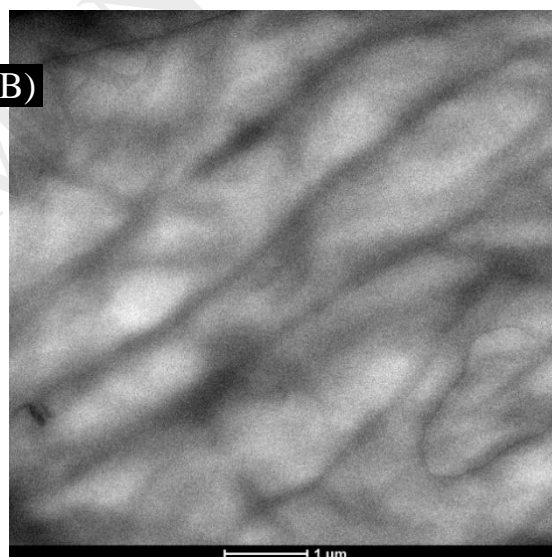
Figure 6 shows the SEM images for PEB/CNC composites of different composition at a lower magnification level, which only allow the observation of the macroscopic phase domains. As can be seen, the morphologies shown in the images obtained for the composites containing up to 20 wt% CNCs (along with Figure 5), indicate the occurrence of a PEB-rich continuous matrix, that would explain the high ductility of the composites obtained within this composition range. On the other hand, the image obtained for the composite containing 40 wt% CNCs shows a non-continuous PEB rich phase constituted by separate domains dispersed within the continuous percolating network. This phase structure would explain the dramatic loss of ductility that is observed when the CNC content exceeds 20 wt%.



**Figure 6.** SEM images of PEB/CNC composites containing 2.5, 5, 20 and 40 wt% CNC with magnification 300x (left) and 1500x (right).

Finally, the dispersion of the CNCs in the PEB matrix has been evaluated by means of TEM (Figure 7). As can be seen, the sample containing 2.5 wt% CNCs shows evenly distributed fine black spots that, according to the observed sizes, can be attributed to both single CNCs and to small CNC aggregates. Anyway, the PEB/CNC composite containing 2.5 wt% CNCs shows a good overall dispersion quality. In addition to the finely dispersed CNCs, the systems containing 5 and 10 wt% CNCs also show the occurrence of large aggregates, indicating some degradation of the dispersion quality. This phenomenon is frequently observed above certain composition (Roy, et al., 2018), and most probably explains the loss of Young's modulus observed in Figure 3 for the composite containing 5 wt% CNCs (relative to the one containing 2.5 wt% CNCs). The observed dispersion degradation should result in mechanical properties below the theoretical expectations (Germiniani, da Silva, Plivelic, & Gonçalves, 2019).

(PEB)



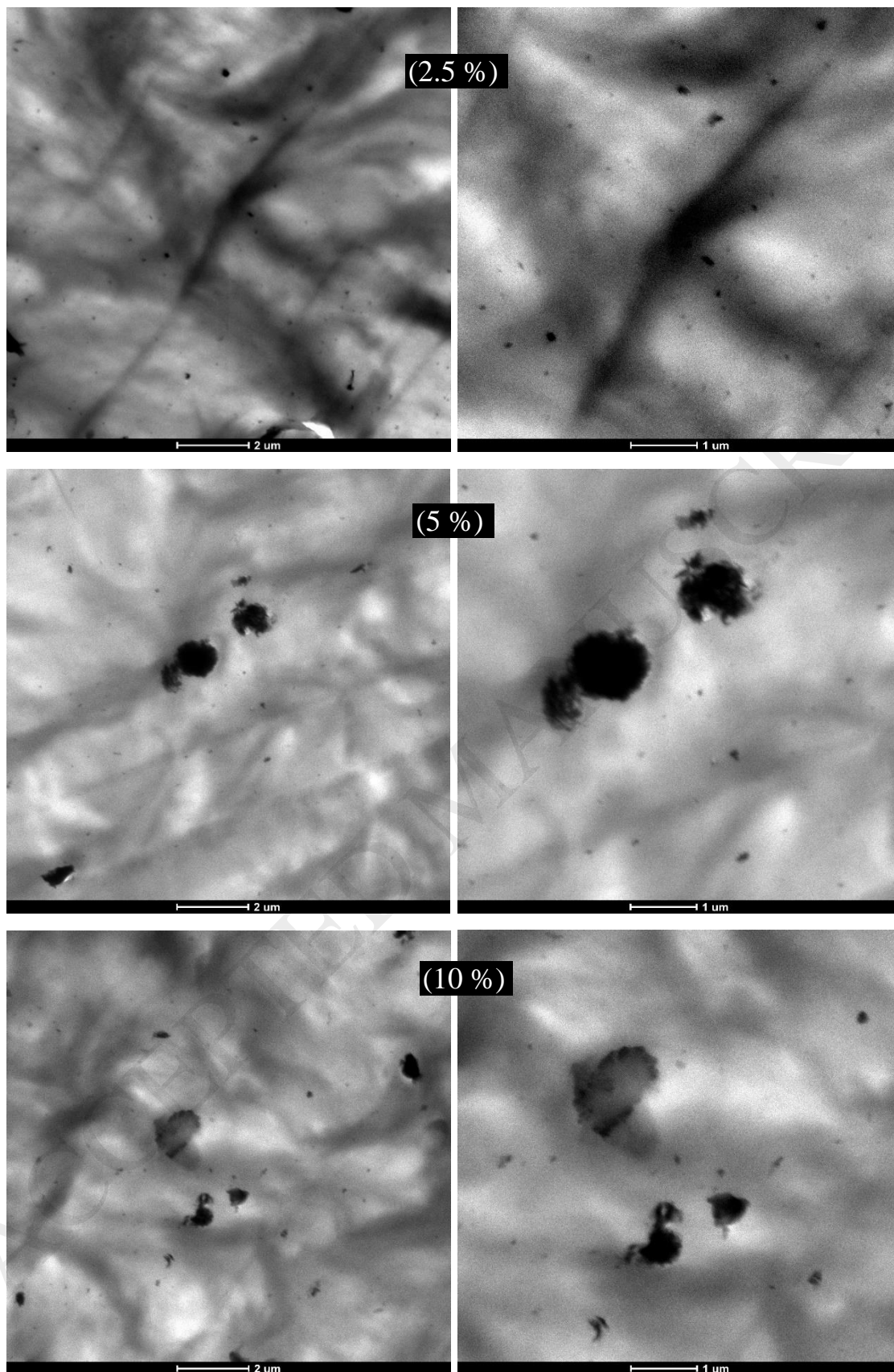


**Figure 7.** TEM images of neat PEB and PEB/CNC composites containing 2.5, 5 and 10 wt% CNC with magnification 3500x (left, 2  $\mu\text{m}$  scale bar) and 6500x (right, 1  $\mu\text{m}$  scale bar).

## 4. Conclusions

The addition of CNCs to PEB results in Polymer Nanocomposites (PNCs) with interesting mechanical properties. Addition of CNCs below the percolation threshold (CNC contents about 2.5 wt%) improves all the measured mechanical properties, including Young modulus, yield stress, stress at break and strain at break. The material improves both resistant and toughness properties. This combination is not easy to achieve, since the addition of CNCs to thermoplastic polymers usually increases the resistant properties at the expense of the ductility of the sample (Habibi, Lucia, & Rojas, *Cellulose Nanocrystals: Chemistry, Self-Assembly, and Applications*, 2010,). The good combination of overall properties is attributable to the presence of a PEB-rich continuous phase responsible for the excellent plastic properties of the materials. In addition, grafting reactions occurring during the melt processing step might also contribute to the good cohesion between matrix and reinforcement.

At higher CNC contents, the CNCs do not achieve an even dispersion, and form a rigid percolating network, resulting from the strong interactions between them. Hence, the reinforcing efficiency decreases. In addition, the domain interconnectivity decreases progressively with the addition of CNCs, and the morphology of the PEB-rich matrix turns gradually from continuous to biphasic with unconnected domains, resulting in a decrease of the ductility of the samples. Nevertheless, most of the strain at break is retained for samples containing up to 20 wt% CNCs, resulting in PNCs containing high reinforcement loads with good overall properties. On the other hand, the Young modulus increases continuously with the addition of CNCs within the composition range investigated in this work (up to 50 wt% CNCs).

Finally, the presence of PEB affects slightly the thermal stability of the CNCs, reducing their degradation temperature to about 250 °C. This result should be taken into account during processing operations.

**Acknowledgements**

The authors are thankful for funds from the Basque Government, Department of Education (IT-927-16) and from the Spanish Ministry of Innovation and Competitiveness MINECO (MAT2016-78527-P).

ACCEPTED MANUSCRIPT

## References

- Azzi Samir, M., Alloin, F., & Dufresne, A. (2005). Review of Recent Research into Cellulosic Whiskers, Their Properties and Their Application in Nanocomposite Field. *Biomacromolecules*, *6*, 612-626.
- Bayati, F., Boluk, Y., & Choi, P. (2014). Diffusion Behavior of Water at Infinite Dilution in Hydroxypropyl Xylan Films with Sorbitol and Cellulose Nanocrystals. *ACS Sustainable Chem. Eng.*, *2*, 1305-1311.
- Beaumont, M., König, J., Opietnik, M., Potthast, A., & Rosenau, T. (2017). Drying of a cellulose II gel: effect of physical modification and redispersibility in water. *Cellulose*, *24*, 1199-1209.
- Boujemaoui, A., Cobo Sanchez, C., Engström, J., Bruce, C., Fogelström, L., Carlmark, A., & Malmström, E. (2017). Polycaprolactone Nanocomposites Reinforced with Cellulose Nanocrystals Surface-Modified via Covalent Grafting or Physisorption: A Comparative Study. *ACS Appl. Mater. Interfaces*, *9*, 35305-35318.
- Cama, G., Mogosanu, D., Houben, A., & Dubruel, P. (2017). Synthetic biodegradable medical polyesters: Poly- $\epsilon$ -caprolactone. In X. Zhang (Ed.), *Science and Principles of Biodegradable and Bioresorbable Medical Polymers. Materials and Properties* (pp. 79–105). Belgium: Woodhead Publishing.
- Chen, P., Cho, S., & Jin, H.-J. (2010). Modification and Applications of Bacterial Celluloses in Polymer Science. *Macromol. Res.*, *18*, 309-320.
- Clasen, C., Sultanova, B., Wilhelms, T., Heisig, P., & Kulicke, W.-M. (2006). Effects of Different Drying Processes on the Material Properties of Bacterial Cellulose Membranes. *Macromol. Symp.*, *244*, 48–58.
- Dhar, P., Tarafder, D., Kumar, A., & Katiyar, V. (2015). Effect of cellulose nanocrystal polymorphs on mechanical, barrier and thermal properties of poly(lactic acid) based bionanocomposites. *RSC Adv.*, *5*, 60426-60440.
- Dong, H., Strawhecker, K., Snyder, J., Orlicki, J., Reiner, R., & Rudie, A. (2012). Cellulose nanocrystals as a reinforcing material for electrospun poly(methyl methacrylate) fibers: Formation, properties and nanomechanical characterization. *Carbohydr. Polym.*, *87*, 2488-2495.
- Dufresne, A. (2017). *Nanocellulose: From Nature to High Performance Tailored Materials*. Walter de Gruyter GmbH.
- Fernández, J., Amestoy, H., Sardon, H., Aguirre, M., Larrañaga, A., & Sarasua, J. (2016). Effect of molecular weight on the physical properties of poly(ethylene brassylate) homopolymers. *J. Mech. Behav. Biomed. Mater.*, *64*, 209-219.
- Fernández, J., Larrañaga, A., Etxeberria, A., & Sarasua, J.-R. (2016). Ethylene brassylate-co- $\delta$ -hexalactone biobased polymers for application in the medical field: synthesis, characterization and cell culture studies. *RSC Advances*, *6*, 22121-22136.
- Fernández, J., Montero, M., Etxeberria, A., & Sarasua, J. (2017). Ethylene brassylate: Searching for new comonomers that enhance the ductility and biodegradability of polylactides. *Polym. Degrad. Stab.*, *137*, 23-34.
- Foster, E., Moon, R., Agarwal, U., Bortner, M., Bras, J., Camarero-Espinosa, S., . . . Youngblood, J. (2018). Current characterization methods for cellulose nanomaterials. *Chem. Soc. Rev.*, *47*, 2609-2679.

- George, M., Shen, W.-Z., Sharma, K., & Montemagno, C. (2017). Characterization of cellulose nanocrystals from a pilot scale facility: the effect of a pretreatment stage and different drying methods. *Cellulose Chem. Technol.*, *51*, 681-691.
- Germiniani, L., da Silva, L., Plivelic, T., & Gonçalves, M. (2019). Poly( $\epsilon$ -caprolactone)/cellulose nanocrystal nanocomposite mechanical reinforcement and morphology: the role of nanocrystal pre-dispersion. *J. Mater. Sci.*, *54*, 414-426.
- Habibi, Y., & Dufresne, A. (2008). Highly Filled Bionanocomposites from Functionalized Polysaccharide Nanocrystals. *Biomacromolecules*, *9*, 1974-1980.
- Habibi, Y., Goffin, A., Schiltz, N., Duquesne, E., Dubois, P., & Dufresne, A. (2008). Bionanocomposites based on poly( $\epsilon$ -caprolactone)-grafted cellulose nanocrystals by ring-opening polymerization. *J. Mater. Chem.*, *18*, 5002-5010.
- Habibi, Y., Lucia, L., & Rojas, O. (2010.). Cellulose Nanocrystals: Chemistry, Self-Assembly, and Applications. *Chem. Rev.*, *110*, 3479–3500.
- Hoeger, I. (2017). Microscopic Analysis of Cellulose Nanofibril (CNF)- and Cellulose Nanocrystal (CNC)-Based Nanocomposites. In H. Kargarzadeh, I. Ahmad, S. Thomas, & A. Dufresne (Eds.), *Handbook of Nanocellulose and Cellulose Nanocomposites* (Vol. 1, pp. 365-392). Wiley.
- Ji, X., Jing, J., Jiang, W., & Jiang, B. (2002). Tensile Modulus of Polymer Nanocomposites. *Polym. Eng. Sci.*, *42*, 983-993.
- Jiang, L., Morelius, E., Zhang, J., Wolcott, M., & Holbery, J. (2008). Study of the Poly(3-hydroxybutyrate-co-3-hydroxyvalerate)/Cellulose Nanowhisker Composites Prepared by Solution Casting and Melt Processing. *J. Compos. Mater.*, *42*, 2629-2645.
- Khoshkava, V., & Kamal, M. (2014). Effect of drying conditions on cellulose nanocrystal (CNC) agglomerate porosity and dispersibility in polymer nanocomposites. *Powder Technol.*, *261*, 288-298.
- Kumar, S., Benicewicz, B., Vaia, R., & Winey, K. (2017). 50th Anniversary Perspective: Are Polymer Nanocomposites Practical for Applications? *Macromolecules*, *50*, 714-731.
- Lee, K.-Y., Tammelin, T., Schulfert, K., Kiiskinen, H., Samela, J., & Bismarck, A. (2012). High Performance Cellulose Nanocomposites: Comparing the Reinforcing Ability of Bacterial Cellulose and Nanofibrillated Cellulose. *ACS Appl. Mater. Interfaces*, *4*, 4078–4086.
- Lezcano, E., Salom Coll, C., & Prolongo, M. (1996). Melting behaviour and miscibility of poly( $\epsilon$ -caprolactone) + poly(4-hydroxystyrene) blends. *Polymer*, 3603-3609.
- Lin, N., & Dufresne, A. (2014). Nanocellulose in biomedicine: Current status and future prospect. *Eur. Polym. J.*, *59*, 302-325.
- Lizundia, E., Meaurio, E., & Vilas, J. (2016). Grafting of Cellulose Nanocrystals. In D. Puglia, E. Fortunati, & J. Kenny (Eds.), *Multifunctional Polymeric Nanocomposites Based on Cellulosic Reinforcements* (pp. 61-113). Oxford: William Andrew.
- Lo Re, G., Engström, J., Wu, Q., Malmström, E., Gedde, U., Olsson, R., & Berglund, L. (2018). Improved Cellulose Nanofibril Dispersion in Melt-Processed Polycaprolactone Nanocomposites by a Latex-Mediated Interphase and Wet Feeding as LDPE Alternative. *ACS Appl. Nano Mater.*, *1*, 2669-2677.
- Mihrianyan, A. (2011). Cellulose from cladophorales green algae: From environmental problem to high- tech composite materials. *J. Appl. Polym. Sci.*, *119*, 2449-2460.

- Ngo, T.-D., Danumah, C., & Ahvazi, B. (2018). Production of Cellulose Nanocrystals at InnoTech Alberta. In K.-Y. Lee (Ed.), *Nanocellulose and Sustainability: Production, Properties, Applications, and Case Studies* (pp. 269-287). Boca Raton: CRC Press.
- Pascual, A., Sardon, H., Veloso, A., Ruipérez, F., & Mecerreyes, D. (2014). Organocatalyzed Synthesis of Aliphatic Polyesters from Ethylene Brassylate: A Cheap and Renewable Macrolactone. *ACS Macro Lett.*, *3*, 849-853.
- Peng, Y., Gardner, D., & Han, Y. (2012). Drying cellulose nanofibrils: in search of a suitable method. *Cellulose*, *19*, 91-102.
- Pezzin, A., Alberda van Ekenstein, G., & Duek, E. (2001). Melt behaviour, crystallinity and morphology of poly(p-dioxanone). *Polymer*, *42*, 8303-8306.
- Pranger, L., & Tannenbaum, R. (2008). Biobased Nanocomposites Prepared by In Situ Polymerization of Furfuryl Alcohol with Cellulose Whiskers or Montmorillonite Clay. *Macromolecules*, *41*, 8682-8687.
- Qin, X., Xia, W., Sinko, R., & Keten, S. (2015). Tuning Glass Transition in Polymer Nanocomposites with Functionalized Cellulose Nanocrystals through Nanoconfinement. *Nano Lett.*, *15*, 6738-6744.
- Reid, M., Villalobos, M., & Cranston, E. (2017). Benchmarking Cellulose Nanocrystals: From the Laboratory to Industrial Production. *Langmuir*, *33*, 1583-1598.
- Roman, M., & Winter, W. (2004). Effect of Sulfate Groups from Sulfuric Acid Hydrolysis on the Thermal Degradation Behavior of Bacterial Cellulose. *Biomacromolecules*, *5*, 1671-1677.
- Roohani, M., Habibi, Y., Belgacem, N., Ebrahim, G., Karimi, A., & Dufresne, A. (2008). Cellulose whiskers reinforced polyvinyl alcohol copolymers nanocomposites. *Eur. Polym. J.*, *44*, 2489-2498.
- Roy, D., Kotula, A., Natarajan, B., Gilman, J., Fox, D., & Migler, K. (2018). Effect of cellulose nanocrystals on crystallization kinetics of polycaprolactone as probed by Rheo-Raman. *Polymer*, *153*, 70-77.
- Sanchez-Rexach, E., Martínez de Arenaza, I., Sarasua, J., & Meaurio, E. (2016). Antimicrobial poly( $\epsilon$ -caprolactone)/thymol blends: Phase behavior, interactions and drug release kinetics. *Eur. Polym. J.*, *83*, 288-299.
- Siqueira, G., Bras, J., & Dufresne, A. (2009). Cellulose Whiskers versus Microfibrils: Influence of the Nature of the Nanoparticle and its Surface Functionalization on the Thermal and Mechanical Properties of Nanocomposites. *Biomacromolecules*, *10*, 425-432.
- Ten, E., Bahr, D., Li, B., Jiang, L., & Wolcott, M. (2012). Effects of Cellulose Nanowhiskers on Mechanical, Dielectric, and Rheological Properties of Poly(3-hydroxybutyrate-co-3-hydroxyvalerate)/Cellulose Nanowhisiker Composites. *Ind. Eng. Chem. Res.*, *51*, 2941-2951.
- Vaia, R., & Wagne, H. (2004). Framework for nanocomposites. *Mater. Today*, *7*, 32-37.
- Xu, X., Liu, F., Jiang, L., Zhu, J., Haagensohn, D., & Wiesenborn, D. (2013). Cellulose Nanocrystals vs. Cellulose Nanofibrils: A Comparative Study on Their Microstructures and Effects as Polymer Reinforcing Agents. *ACS Appl. Mater. Interfaces*, *5*, 2999-3009.
- Yu, H., Qin, Z., Yan, C., & Yao, J. (2014). Green Nanocomposites Based on Functionalized Cellulose Nanocrystals: A Study on the Relationship between Interfacial Interaction and Property Enhancement. *ACS Sustainable Chem. Eng.*, *2*, 875-886.
- Yuan, Y., & Ruckenstein, E. (1998). Miscibility and transesterification of phenoxy with biodegradable poly(3-hydroxybutyrate). *Polymer*, *39*, 1893-1897.

Zuza, E., Meaurio, E., Etxeberria, A., & Sarasua, J. (2006). Exothermal Process in Miscible Polylactide/Poly(vinyl phenol) Blends: Mixing Enthalpy or Chemical Reaction? *Macromol. Rapid Commun.*, 27, 2026-2031.

ACCEPTED MANUSCRIPT